Faraday Discussions

Cite this: *Faraday Discuss.*, 2026, **262**, 248

ROYAL SOCIETY OF CHEMISTRY

PAPER

View Article Online
View Journal | View Issue

Unleashing the power of non-toxic Zn-guanidine catalysts for sustainable lactide polymerization through smart modeling†

Jinbo Ke, ‡[a] Niclas Conen,‡[b] Filip Latz,[b] Jan Niclas Neumann,[a] Martin Fuchs,[a] Alexander Hoffmann, [a] Andreas Jupke*[b] and Sonja Herres-Pawlis *[a]

Received 28th April 2025, Accepted 21st July 2025
DOI: 10.1039/d5fd00062a

Polylactide (PLA) is one of the most promising bioplastics and is therefore often quoted as a solution to fight today's global plastics crisis. However, current PLA production *via* the ring-opening polymerization (ROP) of lactide is not yet sustainable since it heavily relies on the toxic catalyst tin octoate. To overcome the hurdles in scale-up and to accelerate the transition of promising new non-toxic alternative ROP catalysts from laboratory to industry, model-based analysis is a highly effective tool. Herein, our previously introduced kinetic model for the ROP of L-lactide using a non-toxic and robust Zn guanidine "asme"-type catalyst under industrially relevant melt conditions is expanded upon using two new co-initiators. The experimental data is evaluated using "traditional" kinetic analysis following pseudo-first-order kinetics to approximate a relationship between co-initiator concentration and the rate of polymerization. The range of validity of these findings is considerably expanded by taking model data into account to compare the performance of the different co-initiators in lactide ROP.

Introduction

Plastics have become indispensable across modern society due to their exceptional versatility, low-cost production, and adaptability to a wide range of applications. From packaging and construction materials to medical devices and electronics, plastics offer lightweight, durable, and mouldable solutions to countless industries.[1] However, these benefits come at a significant cost. Most conventional plastics are derived from non-renewable fossil resources and are resistant to natural degradation, leading to their persistent accumulation in

[a]*Institute of Inorganic Chemistry, RWTH Aachen University, Landoltweg 1A, 52074 Aachen, Germany. E-mail: sonja.herres-pawlis@ac.rwth-aachen.de*

[b]*Fluid Process Engineering (AVT.FVT), RWTH Aachen University, Forckenbeckstraße 51, 52074 Aachen, Germany. E-mail: andreas.jupke@avt.rwth-aachen.de*

† Electronic supplementary information (ESI) available. See DOI: **https://doi.org/10.1039/d5fd00062a**

‡ These authors contributed equally to this work.

terrestrial and marine environments.[2–4] Furthermore, growing evidence links microplastics to adverse health effects in both wildlife and humans, the long-term impact of which has yet to be determined.

In light of these challenges, PLA has emerged as a promising alternative to petroleum-based plastics. Derived from biological resources, PLA is biodegradable, biocompatible, and holds the potential to compete economically with conventional polymers.[5,6] Among the various synthesis routes, ring-opening polymerization (ROP) of lactide is the preferred method for PLA production. This approach allows for the generation of high-molecular-mass polymers with controlled tacticity and low dispersity, which are crucial for tailoring material properties.[7–9] Moreover, ROP proceeds without the need for solvents or by-product removal, thereby simplifying the downstream processing and reducing the environmental burden typically associated with polymer production.

In industrial production of PLA, the metal-complex-catalysed ROP is the preferred procedure, and the produced polymer tacticity and its molar mass can be controlled.[7–9] Standardly, tin octoate ($Sn(Oct)_2$) combined with an alcohol (co-initiator) is used as the catalyst at industrial scale.[10] However, $Sn(Oct)_2$ is toxic, and traces remain in the polymer after ROP, which can be accumulated in the environment during biodegradation of PLA.[11–13] Therefore, the focus of ongoing research has been shifted to developing non-toxic metal-based catalysts. Numerous studies have been conducted that present non-toxic alternatives for ROP of lactide based on metals such as Mg, Al, Fe, Zn, Ge, Sc and others.[14–43] Among these catalysts, zinc-based systems are especially attractive, due to high activity, availability and low cost of Zn.[30,44–68] Various zinc-based catalysts have been reported to activate ROP of lactide, exceeding the activity of $Sn(Oct)_2$, but the required reaction conditions, additional solvents, low temperature, an inert atmosphere and a purified monomer feed, are at odds with industrial scale.[49,51,52,54,56,59–67,69–71] Therefore, robust, non-toxic and highly active catalysts are needed that can handle these industrially important requirements.[72] Herres-Pawlis *et al.* reported several robust Zn-based catalysts combined with various bis- and hybrid guanidine ligands used under industrially relevant conditions.[55,73–76] Besides the metal-based catalysts, co-initiators (co-Is) play an equally important role in the ROP of lactide on both lab and industry scale.[28,77,78] The deliberate addition of these external nucleophilic co-initiators leads to increased control of the molar mass of the polymer. Furthermore, due to the assistance of co-initiators, the synthesis of complicated polymer architectures and co-polymers is enabled.[49,77] Different types of alcohol with various lengths or branches have been described as co-initiators for the ROP of lactide.[28,43,49,77,79–86] For the industrial application of these catalysts combined with co-initiators, detailed model-based investigations of the behaviour of catalysts on the lab scale is needed. Recently, we developed a mathematical model for describing the ROP of lactide catalyzed by "asme"-type zinc catalysts.[87] In the literature, a second-order rate law is commonly used to describe the ROP of lactide (eqn (1)). Under the assumption that either a coordination–insertion mechanism (CIM) or an activated-monomer mechanism (AMM) takes place, this can be simplified to a pseudo-first-order rate law (eqn (2)), since in the ideal case, the catalyst concentration is constant in both mechanisms. This results in the following equations for the reaction rate (ν) with [LA] being the concentration of the

monomer, [Cat] the catalyst concentration, k_p the rate constant of polymerization, and the observable reaction rate constant k_{obs} is the product of [k_p] and [Cat].[76]

$$v = \frac{-d[LA]}{dt} = k_p \times [Cat] \times [LA] \quad (1)$$

$$v = \frac{-d[LA]}{dt} = k_{obs} \times [LA] \quad (2)$$

Note, that in lactide ROP it is oftentimes not distinguished between catalyst and initiator and both terms are used synonymously in the literature.[76] After integration and transformation of eqn (2) the linearized eqn (3) is obtained.

$$\ln\left(\frac{[LA]_0}{[LA]_t}\right) = k_{obs} \times t \quad (3)$$

As shown in Fig. 3, this gives k_{obs} as the slope of the semilogarithmic plot of monomer consumption *vs.* the time $\left(\ln\left(\frac{[LA]_0}{[LA]_t}\right), t\right)$.

From the slope of a plot of the resulting k_{obs} *vs.* [Cat] the reaction rate constant k_p is then obtained, which allows for the comparison of the performance of different polymerization catalysts (Fig. 4).

However, this textbook-like method has its limitations and does not cover phenomena during ROP that might decrease the reaction rate, like initiation *via* ligands or catalyst decomposition.[84] Note, that it is also not possible to distinguish between CIM and AMM using this method and certain catalysts might promote both mechanisms simultaneously in concurrent reactions. As Fuchs further showed for lactide ROP with a Zn-guanidine catalyst, both the experimental effort and the resource consumption necessary for classic kinetic analysis drastically increase if industrially active co-initiators are added to the reaction system.[87] Hence, a straight-forward method is needed to incorporate co-initiators into the kinetic analysis of lactide ROP to enable a translation of promising new, non-toxic catalysts from lab to industry. As demonstrated previously, due to the increased material investment of the described classical kinetic analysis, model-based methods are a much-needed tool to improve the multivariate understanding of the kinetics of such ROP catalysts (*e.g.* varying catalyst and initiator concentration, temperature, *etc.*).[87]

Building on our approach for catalysing lactide ROP using non-toxic zinc-"asme" catalysts, this work expands both the experimental and modelling aspects of the catalytic system. Specifically, we introduce and investigate the use of bifunctional co-initiators carrying two hydroxyl groups, in contrast to the monofunctional variants employed previously. These bifunctional co-initiators enable the propagation reaction to proceed from both ends of the polymer chain, theoretically allowing for faster monomer conversion compared to using a mono-functional co-initiator. The influence of these bifunctional co-initiators on polymer growth will be systematically studied and incorporated into an expanded kinetic model, enabling a more precise, model-based description of the polymerization process. Ultimately, this advancement aims to broaden the applicability of our catalytic system under industrially relevant conditions while

decreasing the amount of catalyst and improving control over key material characteristics, such as molecular mass and dispersity.

Experimental

Ring-opening polymerization of L-lactide

In a glovebox (MBRAUN), L-lactide (8.0 g, 55.5 mmol), phenyl-1,4-dimethanol, if used as the co-initiator, and the catalyst were weighed according to the respective monomer-to-co-initiator-to-catalyst ratio ([LA]/[co-I]/[Cat] ratio). All exact weighed amounts are listed in Table S1 in the ESI.† The solid reactants were combined and homogenized using an agate mortar. The mixture was transferred to a screw cap vial and removed from the glovebox. A stainless-steel reactor equipped with a precision overhead stirrer ("minisprint PRE1946 – Premex Reactor AG, torque = 20 N cm), a Raman probe (sapphire lens, $d = 0.1$ mm) and a temperature probe were used for all polymerization experiments (see Fig. S1†). The polymerization was monitored *via* Raman spectroscopy using a Kaiser Optical System RXN1 spectrometer with an Invictus NIR Diode Laser (wavelength 785 nm, 450 mW) combined with a TE Cooled 1024 CCD Detector. The reactor was preheated to the reaction temperature of $T = 150$ °C for at least 1 h prior to the polymerization experiments and flushed with Ar (3×). The solid reaction mixture was transferred to the reactor using Ar counter flow. If used as the co-initiator, 1-hexanol was added to the reactor using a Hamilton syringe according to the respective [La]/[co-I]/[Cat] ratio (Tables S1–S5†). The reactor was closed, and the Raman measurement was started, which marks the start of the polymerization ($t = 0$). After the desired reaction time of 90 min, the measurement was stopped. The crude polymerization mixture was analysed using ^{1}H NMR spectroscopy to determine the polymer yield. For further analysis, a sample of the crude product was dissolved in DCM (2.0 ml) and precipitated from EtOH (200.0 ml) and dried in high vacuum. The molar mass and the dispersity of the polymer was determined using a Viscotek GPCmax VE-2001 system combined with a VE-3580 refractive index detector, an HPLC pump and a Viscotek 270 Dual Detector viscosimeter. Two Viscotek T columns (styrene–divinylbenzene-copolymer, pore size between 500 Å and 5000 Å) were used as the stationary phase. THF was used as the mobile phase at a flow rate of 1 ml min^{-1} with the sample concentration ranging between 5 to 7 g l^{-1}. A conventional calibration based on polystyrene standards was used. To access the molar mass of PLA, the obtained molar masses were corrected by a factor of 0.58 according to the literature.[88] The obtained Raman data was assessed using the software *Peaxact* (V4.0 or higher) by *S-PACT.* The characteristic signals of lactide (656 cm^{-1}) and PLA (872 cm^{-1}) were evaluated to determine the reaction rate constant of the polymerization (k_p) as described above.

Ring-opening polymerization of L-lactide in Schlenk tubes

In a glovebox (MBRAUN), L-lactide, *p*-methylbenzyl alcohol, used as the co-initiator, and zinc chloride, used as the catalyst, were weighed depending on the monomer-to-co-initiator-to-catalyst ratio ([LA]/[co-I]/[Cat] ratio = 2500 : 10 : 1) and completely mixed in an agate mortar. The exact amounts are listed in Table S1 in the ESI.† The solid mixture was divided evenly (approximately 500 mg per portion), and each portion was transferred into a Schlenk tube containing

a magnetic stirrer (15 × 4.5 mm). Then the loaded Schlenk tube was heated in an oil bath (150 °C) and the stirring speed was set to 260 rpm. After the desired reaction time, the corresponding tube was removed from the oil bath and cooled under a water flow to stop the polymerization. To determine the polymer yield, the crude product was dissolved in DCM (2.0 ml), an aliquot was transferred to a NMR tube, dried under high vacuum, and a ^{1}H-NMR spectrum recorded.

Results and discussion

Classical analysis of the experimental results

Analogous to our previous study, the "asme"-type complex [$ZnCl_2$(TMGasme)] (**C1**) was chosen as the catalyst for lactide ROP. **C1** was resynthesized according to the literature procedure reported by Schäfer *et al.*[74]

To further expand our polymerization model, two very different alcohols were chosen as co-initiators for this study (Scheme 1). As guiding principles for the selection of co-initiators, we focused on the potential industrial application with cost and high molar mass of the PLA as indicators, as well as the handling of the co-initiator in the lab. 1-Hexanol (**CoI1**) was chosen as the first candidate, due to its low cost and boiling point of 157 °C, which ensures reliable lab-scale testing at 150 °C (see Experimental). As a second candidate, we selected 1,4-benzenedimethanol (**CoI2**). Due to its solid state of aggregation at room temperature, it is easy to handle while ensuring reliable results. Furthermore, **CoI2** is comparable in its aromatic scaffold to the co-initiator *p*-methylbenzylalcohol from our first study.[87] However, **CoI2** is a diol, which in theory allows the overall chain growth sites to be doubled as well.

For both co-initiators, ROP of L-lactide was performed at different [LA]/[co-I]/[Cat] ratios. Analogous to our previous work, the [LA]/[Cat] ratios were chosen between 500 : 1 and 1500 : 1 with a common difference of 250. However, considering 1-hexanol (**CoI1**) is a liquid at room temperature, the Hamilton syringe causes a relatively large error if the sample volume of **CoI1** is small, such as at the ratio [LA]/[co-I]/[Cat] = 1500 : 1 : 1. Therefore, larger amounts of 3.31 eq., 6.62 eq., and 10 eq. were used for the system with **CoI1**. In contrast, for the simply weighed solid 1,4-benzenedimethanol (**CoI2**), the equivalences of 1 eq., 5 eq. and 10 eq.

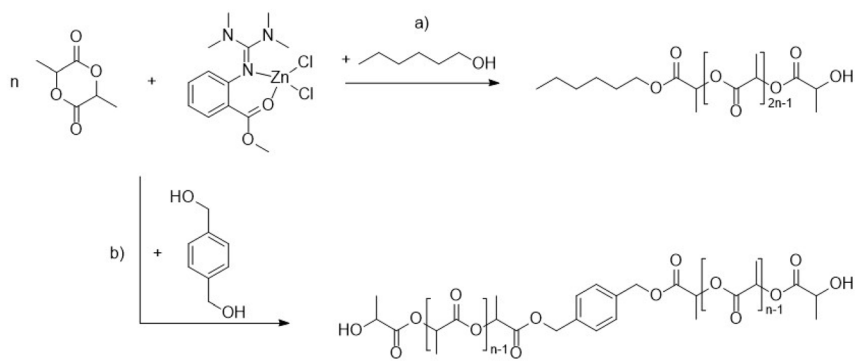

Scheme 1 Lactide ROP catalysed by [$ZnCl_2$(TMGasme)] (**C1**) with two different co-initiators: (a) 1-hexanol (**CoI1**); (b) 1,4-benzenedimethanol (**CoI2**).

were used. Since **CoI2** contains two hydroxyl groups, which provide more reaction sites for lactide ROPs, the [LA]/[Cat] ratios were increased to 2500 : 1, and the corresponding arithmetic difference was up to 500.

To evaluate the influence of **CoI1** and **CoI2** on the ROP, a characterization of the produced polymer by gel permeation chromatography was performed. The measured molar masses were compared with the corresponding theoretical molar masses (ESI†). Table 1 summarizes the whole series of measurements both with and without a co-initiator at a fixed [LA]/[Cat] ratio of 500 : 1. As in our previous study, the concentration of polymer chains is calculated by the sum of the co-initiator and catalyst loadings. Consequently, the molar mass reduces with the increase of co-initiator, as more chain starters are contained in the polymerization mixture.[87] As mentioned above, different batches of L-lactide were used for each co-initiator, which causes a slight deviation due to varying water content. Considering the objective error, the series of measurements with **CoI1** is well matched, as the chains with $M_n = 19\,700$ g mol^{-1} from polymerization with 3.31 eq. **CoI1** were shorter than those without a co-initiator with $M_n = 25\,700$ g mol^{-1}. Herein, the chains obtained from polymerization without a co-initiator were shorter than the theoretical one, probably due to the initiation of chain growth by the "asme"-ligand of **C1** and then decomposition of the catalyst.[74] Increasing the amount of **CoI1** to 6.62 eq. and 10 eq. yielded chains with 10 500 g mol^{-1} and 7800 g mol^{-1}, respectively. For the case of **CoI2**, the chains with 40 600 g mol^{-1} from polymerization with 1 eq. **CoI2** were longer than those without a co-initiator. The small amount of **CoI2** significantly accelerates the catalysis rate and also provides the possibility for the chain to grow in both sites simultaneously, and the conversion of L-lactide is higher; therefore, the chain is longer than in the absence of a co-initiator. The molar mass of chains was decreased to 15 900 g mol^{-1} and 7700 g mol^{-1} with an increase of **CoI2** to 5 eq. and 10 eq. However, the experimental molar mass is not doubled as the theoretical molar mass, which indirectly

Table 1 Comparison between experimental and theoretical molar masses of polymer obtained by L-lactide ROP at the [LA]/[Cat] ratio of 500 : 1 with different co-initiators at different concentrations

		M_n [g mol^{-1}]				
Co-initiator	Eq.	Experimental	Theoretical	Deviation	Mean	$Đ$
—	—	25 700	42 000	−39%	−46%	1.5
		19 000	39 300	−52%		1.7
1-Hexanol (**CoI1**)	3.31	19 700	13 700	44%	60%	1.1
		23 200	13 200	76%		1.3
	6.62	10 500	8500	24%	26%	1.1
		10 800	8500	27%		1.1
	10	7800	6100	28%	30%	1.1
		8200	6200	32%		1.1
1,4-Benzenedimethanol (**CoI2**)	1	40 600	29 400	38%	33%	1.4
		33 400	26 300	27%		1.5
	5	15 900	11 200	42%	42%	1.1
		16 200	11 400	42%		1.1
	10	7700	6300	22%	52%	1.1
		11 300	6200	82%		1.1

illustrates that the activities of the OH groups at both sites of the diol might be different. When the amount of the diol is 10 eq., the result obtained is similar to the case of **CoI1**, in which it can be considered that the amount of **CoI2** approaches saturation. In addition, according to the deviation and the corresponding dispersity, it can be considered that the chain growth could be controlled better with smaller deviation and dispersity in the presence of co-initiators compared to the case without a co-initiator. However, the effect of a co-initiator does not improve linearly with the increasing loading.

With these modified ratios mentioned above, the kinetic evaluation of lactide ROP was performed as described above. Fig. 1 presents the course of the semilogarithmic plot of conversion *vs.* time for a [M]/[co-I]/[Cat] ratio of 500 : 10 : 1 for both **CoI1** and **CoI2**.

As described by eqn (1)–(3), the slope of the semilogarithmic plot gives the apparent pseudo-first-order reaction rate constant k_{obs}. In comparison with our previous study, the curve behaviors of the plot of conversion *versus* time are in good agreement.[87] For both **CoI1** and **CoI2**, the apparent pseudo-first-order reaction rate constant k_{obs} decreased over reaction time. This is most likely caused by the single-site catalytic behavior of **C1** with chain growth initiated by the "asme"-ligand.[74] This competes with the initiation by the external initiator and might cause a self-induced decomposition of the catalyst over the course of the polymerization. Therefore, model-based analysis is also helpful for these chosen co-initiators as will be discussed later.

Nevertheless, herein classic kinetic analysis was performed also at various co-initiator loadings, which is normally not the case in the literature due to the huge amount of necessary experimental work. Furthermore, the obtained data will be used as the experimental support for the development of the analysis model. Due

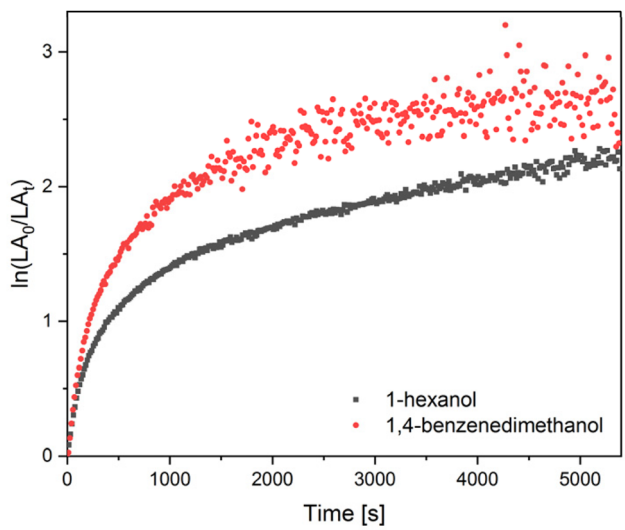

Fig. 1 Semilogarithmic plot of conversion *versus* time of ROP of recrystallized L-lactide with **C1** and 1-hexanol (**CoI1**, black dots) and 1,4-benzenedimethanol (**CoI2**, red dots) at a [LA]/[co-I]/[Cat] ratio of 500 : 10 : 1 at 150 °C with a stirring speed of 260 rpm and a reaction time of 90 min.

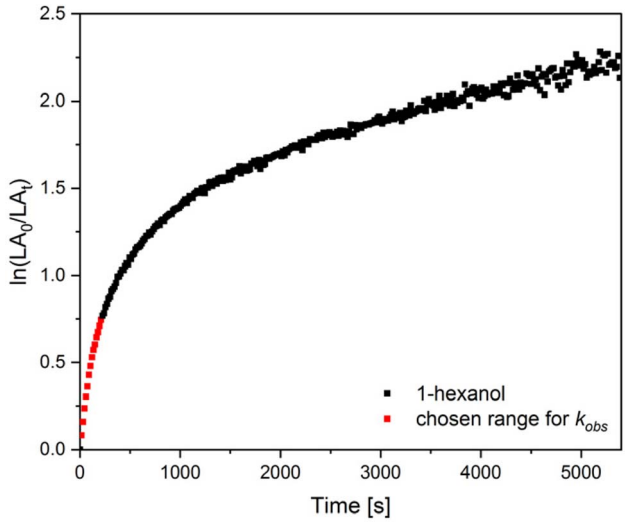

Fig. 2 Semilogarithmic plot of conversion *versus* time of ROP of recrystallized L-lactide with **C1** and 1-hexanol (**Col1**) at a [LA]/[co-I]/[Cat] ratio of 500 : 10 : 1 at 150 °C with a stirring speed of 260 rpm and a reaction time of 90 min.

to the decrease of k_{obs} over time (Fig. 1), only the initial range of the semilogarithmic plot, which shows a linear slope, was used to determine k_{obs} (Fig. 2). Note that due to the approximation the resulting data cannot be taken as absolute values. Therefore, the following kinetic discussion will focus on trends and the given values should not be seen as absolute.

Based on this principle, k_{obs} was determined at different [LA]/[co-I]/[Cat] ratios for both co-initiators (ESI†). As an example, the complete series of measurements

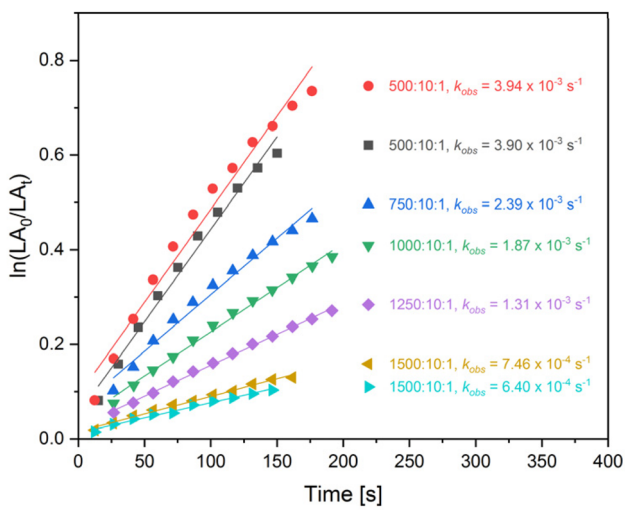

Fig. 3 Semilogarithmic plot of conversion *versus* time of ROP of L-lactide with **C1** and 10 eq. 1-hexanol (**Col1**) to determine the apparent rate coefficient k_{obs} from the initial range.

Table 2 Results of the kinetic evaluation of ROP of L-lactide with **C1** in the presence of different co-initiators

Co-initiator	Equivalence	$k_p \times 10^{-2}$ [L mol^{-1} s^{-1}]
—	—	3.43 ± 0.35
p-Methylbenzylalcohol[89]	1	5.03 ± 0.53
	5	16.3 ± 1.8
	10	26.7 ± 2.8
1-Hexanol (**CoI1**)	3.31	14.9 ± 1.2
	6.62	19.1 ± 1.6
	10	28.7 ± 2.1
1,4-Benzenedimethanol (**CoI2**)	1	11.9 ± 0.70
	5	26.9 ± 0.60
	10	28.4 ± 1.7

with 10 eq. of 1-hexanol (**CoI1**) is shown in Fig. 3. In this case, the polymerizations were carried out at [LA]/[Cat] ratios between 500 : 1 and 1500 : 1.

The determined k_{obs} values were used to determine the reaction rate constant k_p as the slope of a plot of k_{obs} *versus* concentration of catalyst **C1** for the different series of co-initiator loadings (Table 2). According to the results, it can be seen that an increase in co-initiator loading results in a higher k_p-value. This is due to the increased amounts of active sites for polymerization (OH groups). Compared to *p*-methylbenzylalcohol (*p*MeBnOH) which was used previously, **CoI2** containing a similar aromatic scaffold but twice the amount of OH groups allows the catalysis rate to be doubled as well. As expected, the $k_p = (11.9 \pm 0.70) \times 10^{-2}$ L mol^{-1} s^{-1} for **CoI2** was determined, which is doubled as $k_p = (5.03 \pm 0.53) \times 10^{-2}$ L mol^{-1} s^{-1} for *p*MeBnOH under the same conditions with 1 eq. co-initiator (Table 2). Note that for each measurement series of co-initiators, a different batch of lactide as well as **C1** was used, resulting in slight deviations due to varying water content in the monomer.

Although different [LA]/[Cat] ratios were used for **CoI2** (500 : 1 to 2500 : 1 instead of 500 : 1 to 1500 : 1) when compared to **CoI1** and *p*MeBnOH, the determined k_p values in the presence of 10 eq. of co-initiators are comparable within the scope of the error; for **CoI1** $k_p = (28.7 \pm 2.1) \times 10^{-2}$ L mol^{-1} s^{-1}, for *p*MeBnOH $k_p = (26.7 \pm 2.8) \times 10^{-2}$ L mol^{-1} s^{-1} and for **CoI2** $k_p = (28.4 \pm 1.7) \times 10^{-2}$ L mol^{-1} s^{-1}. Furthermore, the catalysis rate can be seen to be significantly greater compared with the k_p value without a co-initiator (Fig. 4). However, in comparison to the k_p values from **CoI1** and *p*MeBnOH with a used quantity of 10 eq., the corresponding k_p value of **CoI2** is similar even though **CoI2** contains twice the amount of OH groups. This indicates that there is an upper limit to the rate-increasing effect of a co-initiator. To visualize the contrast between **CoI1** and **CoI2**, the trend curve of k_p *versus* the added equivalents of the co-initiator is shown in Fig. 5 (left). As can be seen, on the one hand the reaction rate accelerates linearly with an increasing amount of **CoI1**. On the other hand, an even faster increase is observable if the loading of **CoI2** is increased. However, an upper limit is clearly visible resulting in a saturation of the curve. Note that 10 eq. of **CoI2** is equivalent to 20 eq. of OH groups initiating the chain growth. To eliminate the effect of the type of co-initiators on the reaction rate, the k_p values were plotted over the equivalents of OH groups shown in Fig. 5 (right). The trend curves from

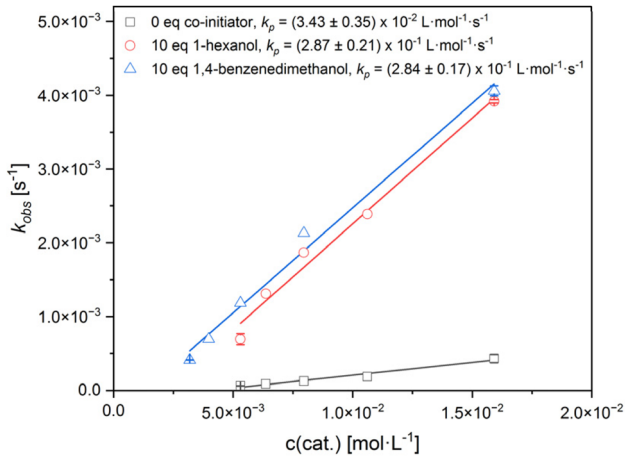

Fig. 4 Determination of the reaction rate constant k_p of ROP of L-lactide with **C1** and 10 eq. 1-hexanol (**CoI1**, red circles) and 1,4-benzenedimethanol (**CoI2**, blue triangles), or without co-initiator (black squares) by plotting the apparent rate coefficient k_{obs} from the initial ranges over the catalyst concentration.

both co-initiators show that an increase in the amount of OH groups to 10 eq. leads to a similar acceleration of reaction rate. Therefore, it can be considered that this is independent of the type of co-initiator. Moreover, the saturation is more clearly visible here, as is the huge added amount of OH groups. It might be that the steric requirement for simultaneous polymerization of multiple sites is not necessarily given, which might prevent the reaction rate from further increasing. This saturation was previously observed in the system that used $Sn(Oct)_2$ as a catalyst, where the mono alcohol used, at more than 20 eq., did not accelerate the reaction rate anymore.[92] Hence it might support the idea that the limit of the co-initiator is independent of the systems with different catalysts; rather it is dependent on the polymerization mechanism.

To verify this conjecture, the investigation of a precise mechanism in the presence of a diol is necessary, as well as the analysis of the influence of 20 eq. of **CoI1** on the reaction rate. However, the classic kinetic analysis as presented above has critical limitations:

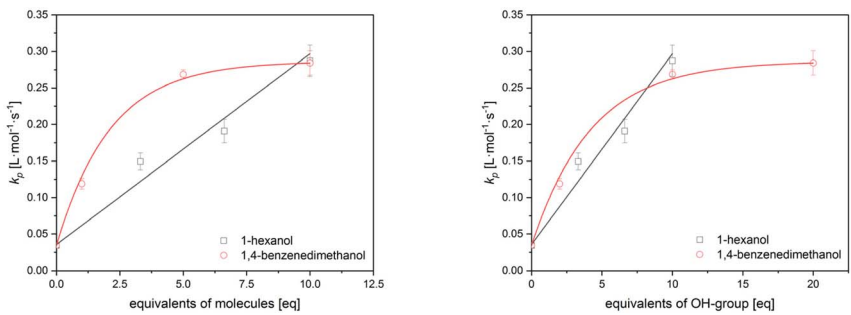

Fig. 5 Plot of the reaction rate constant from the slopes of the initial range *versus* the loading of different co-initiators (left) or the equivalents of OH groups (right).

It requires high amounts of starting compounds needing lots of resources. This is in contrast to sustainable chemistry and therefore the overarching goals of the design of non-toxic ROP catalysts themselves. Additionally, in the case of **C1**, this approach by analyzing k_{obs} and k_p is not an absolute method but rather an approximation. Since the validity range of the determination of k_{obs} is approximated, the method depends strongly on the experimental conditions and resulting data.[73] Therefore, the development of a model-based analysis is necessary for giving a more reliable, unbiased and resource-efficient way to evaluate the performance of these co-initiators for lactide ROP.

Development of a kinetic model for ROP with different co-initiators

The analysis of the experimental data described so far enables a direct comparison of the activity of different catalyst/co-I systems but is not sufficient for prediction of the time course of monomer conversion or prediction of the molar mass distribution. These two key figures are essential for setting optimum operating points in an industrial application. Furthermore, the underlying chemical relationships are to be investigated in greater depth to enable the development of improved catalyst co-initiator systems. For this purpose, a kinetic model is proposed that includes the relevant reactions. As described above, ROP of lactide with the catalyst takes place according to a coordination–insertion mechanism and the ligand of the catalyst can also act as a chain initiator and the catalytically active centre splits off in the process.[74,87] It has already been shown in the literature that zinc alcoholates are also active in the ROP.[90] However, this activity is significantly lower than for the catalyst, which explains why the apparent reaction rate decreases significantly as the reaction progresses.

Based on this finding, the model previously developed by the authors is extended in this work to include the catalytic activity of the metal species formed

(a) Catalyst activation	$D_n + C \underset{k_{C,a2}}{\overset{k_{C,a1}}{\rightleftharpoons}} R_{C,n} + A_C$
	$D_n + CR \underset{k_{CR,a2}}{\overset{k_{CR,a1}}{\rightleftharpoons}} R_{CR,n} + A_{CR}$
(b) Chain initiation	$C + M \xrightarrow{k_{CM}} D_2 + CR$
(c) Propagation	$R_{i,n} + M \underset{k_{i,d}}{\overset{k_{i,p}}{\rightleftharpoons}} R_{i,n+2}$
(d) Chain transfer	$R_{i,n} + R_{j,k} \underset{k_s}{\overset{k_s}{\rightleftharpoons}} R_{i,k} + R_{j,n}$
	$R_{i,n} + D_k \underset{k_s}{\overset{k_s}{\rightleftharpoons}} R_{i,k} + D_n$
(e) Intermolecular transesterification	$R_{i,n} + D_k \underset{k_{te}}{\overset{k_{te}}{\rightleftharpoons}} R_{i,n+k-p} + D_p$
	$R_{i,n} + G_k \underset{k_{te}}{\overset{k_{te}}{\rightleftharpoons}} R_{i,n+k-p} + G_p$
(f) Random chain scission	$R_{i,n} \xrightarrow{k_{de}} R_{i,n-k} + G_k$
	$D_{i,n} \xrightarrow{k_{de}} D_{i,n-k} + G_k$
	$G_{i,n} \xrightarrow{k_{de}} G_{i,n-k} + G_k$

Small molecules:

- C: Catalyst
- CR: Catalyst residue
- M: Monomer
- A_C: Byproduct from catalyst activation
- A_{CR}: Byproduct from catalyst residue activation
- $R_{i,j,0}$: Initiator
- D_0: Alcohol co-initiator

Macromolecules:

- R: Active (reactive) chain
- D: Inactive (dormant) chain
- G: Terminated chain

Indices:

- i: chain end, $\in [C; CR]$
- n, k, p: chain length, $\in [0 \quad \infty]$

Scheme 2 Proposed scheme for the summarised kinetics for ROP of lactide with an "asme"-type catalyst and a monofunctional alcohol as co-initiator.

after the split-off of the catalyst metal centre.[87] Note that, due to the reaction conditions, a clear specification of this less-active species is not possible. Since both $ZnCl_2$ and Zn alkoxide might act as a weak catalyst, a further specification of the active species is not made. Scheme 2 is set up to model the reaction system that uses monofunctional co-initiators.

The nomenclature of the polymer species is based on the literature in this field for the $Sn(Oct)_2$-catalyzed ROP.[91–97] Polymer chains are divided into active (R), inactive (D) and terminated (G) populations. The active chains are divided into chains with a catalyst (C) and chains with a catalyst rest (CR) at the end of the chain. The index of the populations represents the number of repeating units. The lactoyl unit is chosen to enable a more accurate description of trans-esterification reactions.

Reaction (a) describe the activation of the co-initiator (for $n = 0$) or an inactive chain (for $n > 0$) with catalyst or catalyst residue forming an initiator ($n = 0$) or an active chain ($n > 0$) with catalyst or catalyst residue as a chain end. This activation is an equilibrium reaction with equilibrium constant $K_{x,a} = k_{x,a1}/k_{x,a2}$ (x = C, CR). The activation is assumed to be much faster than the chain propagation and is therefore modelled as quasi-instantaneous. This is in accordance with studies for $Sn(Oct)_2$ as the catalyst and can be seen for the "asme"-type catalysts as well since no induction period is visible after the melting of lactide.

Reaction (b) means that, in addition to the activated co-initiator, the ligand of the catalyst can also act as a chain initiator with reaction rate constant k_{CM}. The reaction with a monomer produces an inactive chain with two repeating units with the elimination of a catalyst residue.

Reaction (c) describes the actual propagation of an active chain by reaction with a monomer to form an active chain that is two repeating units longer with the reaction constants $k_{C,p}$ for catalyst at the chain end and $k_{CR,p}$ for catalyst residue at the chain end. The reaction is assumed to be an equilibrium reaction. The equilibrium constant can be calculated from the maximum achievable conversion. For $n = 0$, an initiator molecule starts an active chain with two repeating units.

Reaction (d) describes the chain transfer. This consists of the exchange of active chain ends between active and inactive chains. This reaction has no influence on the monomer conversion but is essential for mapping the molecular mass distribution. Due to the equivalence of forward and reverse reactions, an equilibrium constant of one is assumed.[92]

Reaction (e) describe intermolecular transesterification reactions with the reaction rate constant k_{tr}. These significantly influence the width of the molecular mass distribution. Analogous to the chain-transfer reactions, an equilibrium constant of one is assumed here due to the equivalence of the forward and reverse reactions.

Random chain-scission reactions are represented by the reactions (f). Polymer chains irreversibly break into terminated chains at a random point with the reaction rate constant k_{de}. This reaction is only relevant at elevated temperatures with high thermal stress.

In contrast to the use of a monoalcohol like **CoI1**, there are two activation stages when using a diol as a co-initiator, which are depicted in Scheme 3. The result of the second stage corresponds to the PLA shown in Scheme 1.

1. activation stage $\mathrm{HO{-}R{-}OH + ZnL_n \rightleftharpoons HO{-}R{-}O{-}ZnL_{n-1} + A}$

2. activation stage $\mathrm{HO{-}R{-}O{-}ZnL_{n-1} + ZnL_n \rightleftharpoons L_{n-1}Zn{-}O{-}R{-}O{-}ZnL_{n-1} + A}$

Scheme 3 Reaction equations for two-stage catalyst (ZnL_n) activation with a bifunctional co-initiator.

Both OH groups of the co-initiator can form an active species by ligand exchange with the ligand of the catalyst, splitting off an acid residue. This also leads to polymer chains that can have two active chain ends. Overall, this results in the following more-complex reaction network depicted in Scheme 4.

The reactions now include a second activation step, during which a ligand exchange occurs between the second hydroxyl group of the co-initiator and the

(a) 1. catalyst activation

$$\mathrm{D}_n + \mathrm{C} \underset{\mathrm{k_{C,a2}}}{\overset{\mathrm{2\ k_{C,a1}}}{\rightleftharpoons}} \mathrm{R_{C,n}} + \mathrm{A_C}$$

$$\mathrm{D}_n + \mathrm{CR} \underset{\mathrm{k_{CR,a2}}}{\overset{\mathrm{2\ k_{CR,a1}}}{\rightleftharpoons}} \mathrm{R_{CR,n}} + \mathrm{A_{CR}}$$

2. catalyst activation

$$\mathrm{R}_{i,n} + \mathrm{C} \underset{\mathrm{2\ k_{C,a2}}}{\overset{\mathrm{k_{C,a1}}}{\rightleftharpoons}} \mathrm{R_{i,C,n}} + \mathrm{A_C}$$

$$\mathrm{R}_{i,n} + \mathrm{CR} \underset{\mathrm{2\ k_{CR,a2}}}{\overset{\mathrm{k_{CR,a1}}}{\rightleftharpoons}} \mathrm{R_{i,CR,n}} + \mathrm{A_{CR}}$$

(b) Chain initiation

$$\mathrm{C} + \mathrm{M} \xrightarrow{\mathrm{k_{CM}}} \mathrm{D}_2 + \mathrm{CR}$$

(c) Propagation

$$\mathrm{R}_{i,n} + \mathrm{M} \underset{\mathrm{k_{i,d}}}{\overset{\mathrm{k_{i,p}}}{\rightleftharpoons}} \mathrm{R}_{i,n+2}$$

$$\mathrm{R}_{i,i,n} + \mathrm{M} \underset{\mathrm{2\ k_{i,d}}}{\overset{\mathrm{2\ k_{i,p}}}{\rightleftharpoons}} \mathrm{R}_{i,i,n+2}$$

$$\mathrm{R_{C,CR,n}} + \mathrm{M} \underset{\mathrm{k_{C,d}}}{\overset{\mathrm{k_{C,p}}}{\rightleftharpoons}} \mathrm{R_{C,CR,n+2}}$$

$$\mathrm{R_{C,CR,n}} + \mathrm{M} \underset{\mathrm{k_{CR,d}}}{\overset{\mathrm{k_{CR,p}}}{\rightleftharpoons}} \mathrm{R_{C,CR,n+2}}$$

(d) Chain transfer

$$\mathrm{R}_{i,j,n} + \mathrm{D}_k \underset{\mathrm{k_s}}{\overset{\mathrm{k_s}}{\rightleftharpoons}} \mathrm{R}_{i,j,k} + \mathrm{D}_n$$

$$\mathrm{R}_{i,j,n} + \mathrm{D}_k \underset{\mathrm{k_s}}{\overset{\mathrm{k_s}}{\rightleftharpoons}} \mathrm{R}_{i,k} + \mathrm{R}_{j,n}$$

$$\mathrm{R}_{i,j,n} + \mathrm{R}_{i,k} \underset{\mathrm{k_s}}{\overset{\mathrm{k_s}}{\rightleftharpoons}} \mathrm{R}_{i,j,k} + \mathrm{R}_{i,n}$$

$$\mathrm{R}_{i,n} + \mathrm{R}_{j,k} \underset{\mathrm{k_s}}{\overset{\mathrm{k_s}}{\rightleftharpoons}} \mathrm{R}_{i,k} + \mathrm{R}_{j,n}$$

$$\mathrm{R}_{i,n} + \mathrm{D}_k \underset{\mathrm{k_s}}{\overset{\mathrm{k_s}}{\rightleftharpoons}} \mathrm{R}_{i,k} + \mathrm{D}_n$$

(e) Intermolecular transesterification

$$\mathrm{R}_{i,j,n} + \mathrm{R}_{i,j,k} \underset{\mathrm{k_{te}}}{\overset{\mathrm{k_{te}}}{\rightleftharpoons}} \mathrm{R}_{i,j,n+k-p} + \mathrm{R}_{i,j,p}$$

$$\mathrm{R}_{i,j,n} + \mathrm{R}_{i,k} \underset{\mathrm{k_{te}}}{\overset{\mathrm{k_{te}}}{\rightleftharpoons}} \mathrm{R}_{i,j,n+k-p} + \mathrm{R}_{i,p}$$

$$\mathrm{R}_{i,j,n} + \mathrm{D}_k \underset{\mathrm{k_{te}}}{\overset{\mathrm{k_{te}}}{\rightleftharpoons}} \mathrm{R}_{i,j,n+k-p} + \mathrm{D}_p$$

$$\mathrm{R}_{i,j,n} + \mathrm{G}_k \underset{\mathrm{k_{te}}}{\overset{\mathrm{k_{te}}}{\rightleftharpoons}} \mathrm{R}_{i,j,n+k-p} + \mathrm{G}_p$$

$$\mathrm{R}_{i,n} + \mathrm{D}_k \underset{\mathrm{k_{te}}}{\overset{\mathrm{k_{te}}}{\rightleftharpoons}} \mathrm{R}_{i,n+k-p} + \mathrm{D}_p$$

$$\mathrm{R}_{i,n} + \mathrm{G}_k \underset{\mathrm{k_{te}}}{\overset{\mathrm{k_{te}}}{\rightleftharpoons}} \mathrm{R}_{i,n+k-p} + \mathrm{G}_p$$

(f) Random chain scission

$$\mathrm{R}_{i,j,n} \xrightarrow{\mathrm{k_{de}}} \mathrm{R}_{i,j,n-k} + \mathrm{G}_k$$

$$\mathrm{R}_{i,n} \xrightarrow{\mathrm{k_{de}}} \mathrm{R}_{i,n-k} + \mathrm{G}_k$$

$$\mathrm{D}_{i,n} \xrightarrow{\mathrm{k_{de}}} \mathrm{D}_{i,n-k} + \mathrm{G}_k$$

$$\mathrm{G}_{i,n} \xrightarrow{\mathrm{k_{de}}} \mathrm{G}_{i,n-k} + \mathrm{G}_k$$

Small molecules:

- C: Catalyst
- CR: Catalyst residue
- M: Monomer
- A_C: Byproduct from catalyst activation
- A_{CR}: Byproduct from catalyst residue activation
- $R_{i,j,0}$: Initiator
- D_0: Alcohol co-initiator

Macromolecules:

- R: Active (reactive) chain
- D: Inactive (dormant) chain
- G: Terminated chain

Indices:

- i, j: chain end, $\in [C; CR]$
- n, k, p: chain length, $\in [0 \quad \infty]$

Scheme 4 Proposed scheme for the summarised kinetics for the ROP of lactide with an "asme"-type catalyst and a bifunctional alcohol as co-initiator.

catalyst or catalyst residue. It is important to note that the relevant factor for determining reaction rates is not the concentration of active or inactive chains, but rather the concentration of active or inactive chain ends. This is reflected in the reaction scheme by incorporating a factor of 2 into the reaction rate constant for the forward reaction of the first stage and the reverse reaction of the second stage. Furthermore, active chains must be distinguished not only based on their active end but also according to the number of active ends present. In the scheme provided, this differentiation is achieved using the indices i and j, which represent either a catalyst-bound chain end or a chain end associated with a catalyst residue. This distinction introduces a significant number of additional reactions, including propagation, chain transfer, intermolecular transesterification, and random chain scission, all of which must be accounted for to achieve accurate modeling.

Mathematical description of the reaction systems

The component mass balances for the small molecules and population balances for the polymer species for a batch reactor are drawn up for both reaction systems, assuming an isochoric reaction.[98] This assumption is justified because of the only small differences in density between lactide and PLA. The resulting system of partial differential equations is converted into a system of ordinary differential equations using the method of moments. As suggested in the literature, the specific chain lengths R_1 and R_0 are omitted in the final equations.[91–93] Solving the equation system, one can calculate chain properties including conversion X, number average molecular mass M_n and dispersity $Đ$. The moments of the polymer populations are defined according to the following equation:

$$\mu_i^P = \sum_{n=0}^{\infty} n^i P_n \quad (P = R_{C,C}, R_{C,CR}, R_{CR,CR}, R_C, R_{CR}, D, G) \tag{4}$$

In this equation, P symbolizes any occurring polymeric species, n is the number of repeating units and i the order of the moment.

The moments 0 to 3 are used for the mathematical description of the system. A gamma distribution is assumed for the chain-length distribution. The following relationship can be derived as the closing condition for the calculation of the 3rd moment:[99]

$$\mu_3^P = \frac{\mu_2^P\left(2\mu_2^P\mu_0^P - \left(\mu_1^P\right)^2\right)}{\mu_1^P\mu_0^P} \tag{5}$$

The complete differential equation system of both reaction systems including all mass balances, population balances and moment equations can be found in the ESI.† For the general derivation of moment equations, please refer to the literature.[100,101]

X, M_n and $Đ$ are then calculated using the following equations:

$$X = \frac{M_0 - M}{M_0} \tag{6}$$

$$r_n = \frac{\sum_P \mu_1^P}{\sum_P \mu_0^P} \tag{7}$$

$$M_n = r_n m_{Mon} + m_I \tag{8}$$

$$r_w = \frac{\sum_P \mu_2^P}{\sum_P \mu_1^P} \tag{9}$$

$$Đ = \frac{r_w}{r_n} \tag{10}$$

Here, r_n and r_w represent number and weight average chain length. Note that m_{Mon} is the molar mass of the lactoyl repeating unit. m_I denotes the molecular mass of the initiator species that is formed in the activation step from the reaction of the catalyst and co-initiator.

Parameter estimation

The reaction system described requires the determination of seven unknown reaction parameters that cannot be determined from the literature. To minimize parameter correlation, determination proceeds in a sequential manner through four distinct steps. During all these steps, deviations between experimental data and model data are minimized with a least squares objective function.

Step 1: experiments utilizing $ZnCl_2$ as the catalyst are employed to determine the reaction parameters for activation and propagation with catalyst residues ($k_{CR,p}$, $K_{CR,A}$).

Step 2: a reduced reaction system is utilized to determine the propagation and activation parameters of the ROP with a catalyst (k_{CM}, $k_{C,p}$, $K_{C,A}$). Equations (d) through (f) can be disregarded in this step, as they exert no influence on monomer concentration but merely broaden or shift the molecular mass distribution.

Step 3: the system from step 2 together with reactions (f) are used to determine the kinetic parameter of random chain scission k_{de} by minimizing deviations in the number average molecular mass of the polymer. Intermolecular transesterification reactions can be neglected since they only contribute to symmetrically broadening the molecular mass distribution and therefore do not influence the number average molecular mass.

Step 4: the complete kinetic scheme is used to determine the kinetic parameter of the intermolecular transesterification reaction k_{te} by minimizing deviations in the dispersity of the molecular mass distribution of the polymer.

To enhance parameter identifiability and comparability, it is postulated that chain initiation by the ligand occurs independently of the co-I employed. Consequently, k_{CM} is determined exclusively for *p*-MeBnOH and maintained constant for the other two co-Is. Furthermore, it is assumed that transesterification and chain scission have the same rate constant for all polymer populations.

The systems of differential equations are solved in MATLAB using the *ode15s* solver. Parameter estimations were performed minimizing the respective objective function in MATLAB using the built-in *lsqnonlin* function.

Table 3 Fitted parameter set according to step 1 for $ZnCl_2$ as catalyst for the polymerization of L-lactide at 150 °C with 95% confidence intervals

Parameter	Unit	Value	Lower bound	Upper bound
$k_{CR,p}$	L mol^{-1} s^{-1}	0.0032	0.0014	0.0052
$K_{CR,a}$	—	0.0471	−0.0109	0.0949

Results of the parameter estimation

The resulting kinetic parameters from the parameter estimation for the $ZnCl_2$-catalysed reaction are presented in Table 3. As only one experiment (see Table S1†) was used for parameterisation and the two parameters are strongly correlated, the confidence intervals are comparatively wide. These were assumed to be sufficiently accurate for this work, as the activity of the deteriorated catalyst part is significantly lower than that of the catalyst. Accordingly, this influence is less relevant. In line with this reasoning, the rate constants for $ZnCl_2$-catalysed ROP with the two other co-Is used in this work were not determined.

An overview of all experiments conducted in this work and used for parameterisation and further analysis are shown in Tables S3–S5† (for **CoI1**) and Tables S6–S8† (for **CoI2**). Further experiments used for parameterisation and analysis of *p*-MeBnOH are taken from Conen *et al.* and Fuchs.[87,89] Table 4 lists the kinetic parameters determined according to step 2 for all co-Is tested. In addition, the 95% confidence intervals of the parameter estimates are given to categorise the reliability. Firstly, it can be noted that the values for the propagation rate constant $k_{C,p}$ are of a similar order of magnitude for all co-Is. The equilibrium constant of the catalyst activation $K_{C,a}$ is also very similar for **CoI1** and *p*-MeBnOH,

Table 4 Fitted parameter set according to step 2 for the polymerization of L-lactide with a catalyst at 150 °C with 95% confidence intervals for both co-Is tested and *p*-MeBnOH.[87,89]

Co-initiator	Parameter	Unit	Value	Lower bound	Upper bound
p-MeBnOH	k_{CM}	s^{-1}	581.4	530.9	631.8
	$k_{C,p}$	L mol^{-1} s^{-1}	1.304	1.214	1.394
	$K_{C,a}$	—	2460	2314	2606
CoI1	$k_{C,p}$	L mol^{-1} s^{-1}	1.185	1.169	1.201
	$K_{C,a}$	—	3362	3305	3419
CoI2	$k_{C,p}$	L mol^{-1} s^{-1}	1.079	1.049	1.109
	$K_{C,a}$	—	29 630	28 511	30 750

Table 5 Mean absolute errors of conversion for the parameterisations of all co-Is tested and *p*-MeBnOH.[87,89]

Co-initiator	MAE for conversion
p-MeBnOH	0.039
CoI1	0.057
CoI2	0.056

but the value for the **CoI2** is significantly higher. The confidence intervals are very narrow for all parameters, which indicates a high precision of the parameters for the experimental data used.

The mean absolute errors for the parameterisations regarding the conversion are listed in Table 5.

For all co-Is, the MAE is less than 6%, which indicates an acceptable agreement between experimental data and model. For *p*-MeBnOH as a co-I, this deviation is even less than 4%. A possible explanation for this, in addition to deviations in the accuracy of the experimental data, lies in the procedure used. Since, in contrast to the two other co-Is, the value for k_{CM} was also released as a fit parameter; a more precise adjustment to the experimental data used is possible here due to the model.

The parameters k_{te} and k_{de} relevant for the model-based description of the molecular mass distribution are listed in Table 6 together with the 95% confidence intervals. These parameters were determined using the methodology described in steps 3 and 4. Again, only minor deviations between experimental data and model prediction are recognisable for the dispersity of the molecular mass distribution. The parameters determined for k_{te} are of a similar order of magnitude for all co-Is tested and match findings reported for $Sn(Oct)_2$ as catalyst.[92,93] For all experiments used for parameterisation, the measured dispersities range between 1.05 and 1.3. On one hand, this reduces the reliability of k_{te} for areas with higher dispersities. On the other hand, this demonstrates that with the catalyst co-initiator systems used, the dispersities are in low ranges and therefore the breadth of the distribution for these systems is not particularly problematic.

For the simulative description of the number-average molar mass, on the other hand, there are larger deviations. For **CoI1**, even the determined value for k_{de} becomes 0, since a large number of the measured mean molar masses are already higher than the ones calculated by simulation for $k_{de} = 0$. The uncertainty regarding the parameter estimation is already clear when looking at the confidence intervals, as these contain 0 for all co-Is. However, this is also consistent with literature data that at 150 °C k_{de} assumes low values due to the still comparatively low thermal load[93,95] or is even completely neglected in most publications.[91,92,96] Another factor that may play a role in this phenomenon is the initiation efficiency, as this leads to longer chain lengths than predicted by the model.

Table 7 lists the mean absolute errors of the parameter estimations for number-average molecular mass and dispersity of the molecular mass

Table 6 Fitted parameter set according to steps 3 and 4 for the polymerization of L-lactide with a catalyst at 150 °C with 95% confidence intervals for all co-Is tested and *p*-MeBnOH.[87,89]

Co-initiator	Parameter	Unit	Value	Lower bound	Upper bound
p-MeBnOH	k_{te}	s^{-1}	0.00118	−0.00572	0.00808
	k_{de}	L mol^{-1} s^{-1}	3.99×10^{-7}	-2.37×10^{-6}	3.17×10^{-6}
CoI1	k_{te}	s^{-1}	0.00178	−0.01172	0.01529
	k_{de}	L mol^{-1} s^{-1}	0	—	—
CoI2	k_{te}	s^{-1}	0.00228	−0.0272	0.0317
	k_{de}	L mol^{-1} s^{-1}	8.00×10^{-9}	-1.69×10^{-8}	3.29×10^{-8}

Table 7 Mean absolute errors for the estimation of transesterification and chain scission parameters according to steps 3 and 4 for all co-Is

Co-initiator	MAE for M_n in g mol^{-1}	MAE for $Đ$
p-MeBnOH	5126	0.0365
CoI1	12 649	0.0871
CoI2	6480	0.0648

distribution. As already described, there are sometimes high deviations between the model and experimental data, which is why there are comparatively high deviations in the M_n values. The errors in dispersity, on the other hand, are significantly lower.

In order to gain an initial insight into the suitability of the underlying reaction system for modelling the ROP, the reaction parameters determined from the experiments with a co-I are used for extrapolation to experiments without a co-I. Here, the influence of the chain-start by catalyst is much more pronounced, as this must inevitably take place in order for polymer chains to be formed, which can then grow. Accordingly, this property of the catalysts used must be accurately described for good predictions of the polymerization process. In addition to the comparison of modelling and experimental data, the internal consistency between the modelling of monofunctional and bifunctional co-Is can also be tested here. For a co-I concentration of 0, both model parameterisations for a monofunctional alcohol as co-I and the model for a bifunctional alcohol as co-I should produce an equal conversion curve. Fig. 6 shows this comparison together with experimental data for a [LA]/[Cat] ratio of 500 : 1. There is very little deviation for the two monofunctional co-I models. For the bifunctional co-I model, slight deviations can be recognised both qualitatively and quantitatively, but these are

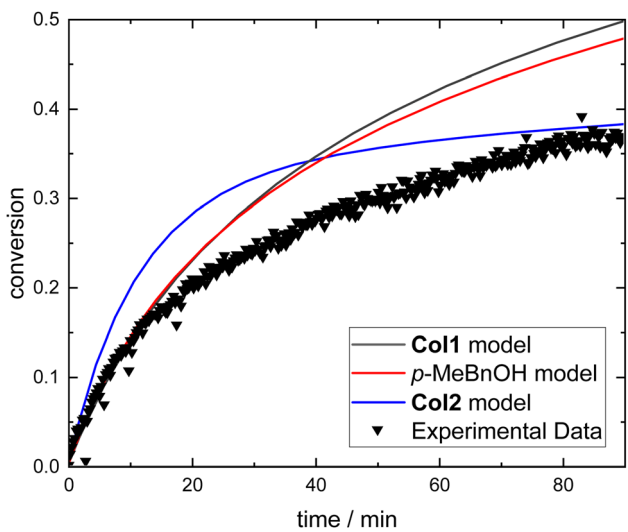

Fig. 6 Comparison of model for all three co-I parameterisations and experimental data for monomer conversion over time for a ratio [LA]/[co-I]/[Cat] of 500 : 0 : 1.

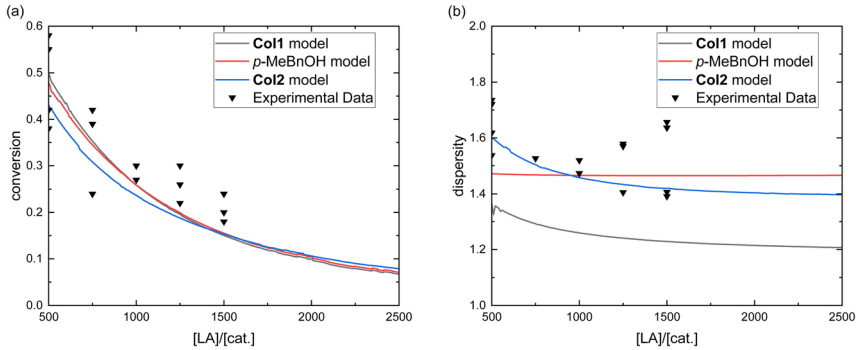

Fig. 7 Comparison of experimental data and model predictions for experiments without a co-I against the ratio of monomer to catalyst concentrations for (a) conversion and (b) dispersity after 90 minutes reaction time. Experimental data for *p*-MeBnOH are taken from Conen *et al.*[87] and Fuchs.[89]

within an acceptable range overall. All models show satisfactory results, especially when compared with experimental data.

Fig. 7 also shows the comparison of models with experimental data for reaction systems without a co-I. In panel (a), the conversion profiles are plotted against the ratio of initial monomer to catalyst concentration ([LA]/[Cat]). Here, the different models should produce identical curve progressions, which is observable with only minor deviations. The comparison with experimental data demonstrates that the extrapolation capability of the models yields acceptable results even outside the concentration ranges used for parameterisation.

Panel (b) shows the same comparison for the dispersity of the molecular mass distribution. The absence of a co-initiator leads to a loss of the controllability over the reaction, which can be seen by the significantly higher dispersities even at lower conversions. Here, the extrapolation capability of the model is significantly more challenging, as the experiments used for parameterisation all had dispersities in the range of 1.05 to 1.3, which is considerably lower than the measured dispersities of 1.4 to 1.8 for the experiments without a co-I. The experimental results are quantitatively matched much less accurately than for the conversion. Nevertheless, it is qualitatively observable that all models predict significantly higher dispersities for initial formulations without a co-I compared to experiments with a co-I, suggesting that the underlying chemical mechanisms are represented qualitatively.

Model-based analysis of the co-initiator influence

Based on the determined kinetic parameters, it can already be concluded that the use of **CoI1** or *p*-MeBnOH only leads to minor differences in the measured conversion and thus also in the suitability for catalyst activation. For the use of **CoI2**, a significant difference to the two previous co-Is can already be determined based on the equilibrium of the catalyst activation. The value of the equilibrium constant of the activation $K_{C,a}$ is significantly higher, whereby considerable advantages in achieving high conversions can be determined, particularly with the "asme"-type catalyst used. The high equilibrium constant has two effects that

both increase the conversion. These can be illustrated using the reaction equations (a) and (b) of the reaction system in Scheme 2. As already described, the catalyst activation in equation (a) is assumed to be quasi-instantaneous, *i.e.*, this reaction is always in equilibrium. The equilibrium of the reaction can be described using the equilibrium constant $K_{C,a}$ as follows:

$$K_{C,a} = \frac{\mu_0^{R_C} \times A_C}{C \times \mu_0^{D}} \tag{11}$$

On one hand, increasing the equilibrium constant increases the concentration of active polymer chains ${\mu_0}^{R_C}$ that can propagate. On the other hand, it reduces the concentration of unbound catalyst C, which in turn leads to a reduced reaction rate of the chain-start by catalyst even at the same value for k_{CM}. The second effect in particular leads to a significant improvement in the potential of "asme"-type catalysts for industrial ROP. Both effects can be seen in Fig. 8 for an initial ratio of [LA]/[co-I]/[Cat] of 500 : 5 : 1. The conversion for the bifunctional co-I increases significantly faster and reaches a higher final value after 90 minutes (a). The two monofunctional co-Is show only minor differences. In (b), it is evident that the ratio of polymer chains with catalyst at the end to initially used catalyst for the bifunctional co-I is considerably higher from the beginning compared to the monofunctional co-Is. This is derived from the first mentioned effect. Additionally, it is noticeable that this ratio decreases more slowly, which can be attributed to the slower chain initiation by the catalyst.

The influence of co-I concentration for all tested co-Is on the conversion after 90 minutes of reaction time is shown in Fig. 9. Overall, acceptable agreements between experimental data and model predictions are observed. All models predict similar values for the reaction system without a co-I. However, with increasing co-I concentration, the predicted conversions for the bifunctional co-I increase significantly and reach the equilibrium conversion of the polymerization already at 5 co-I equivalents. For the two monofunctional co-Is, this would only be achieved at about 25 co-I equivalents. The decisive factors for this effect are again the previously described effects due to the increased equilibrium constant of catalyst activation.

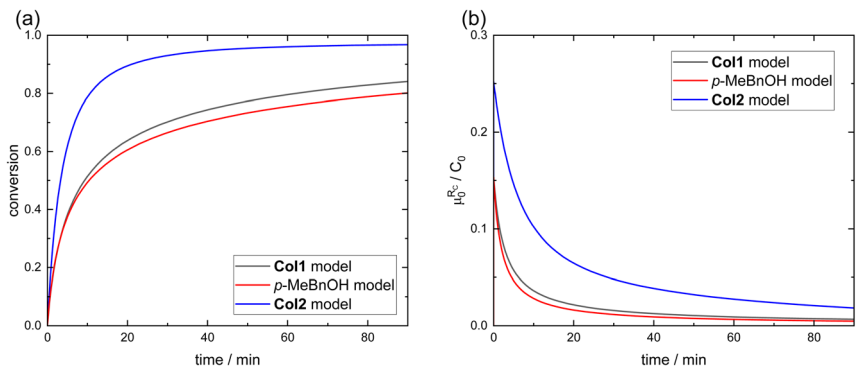

Fig. 8 Effects of higher activation equilibrium constants on (a) conversion and (b) ratio of active chains with catalyst-end to initial catalyst concentration over time for 90 minutes.

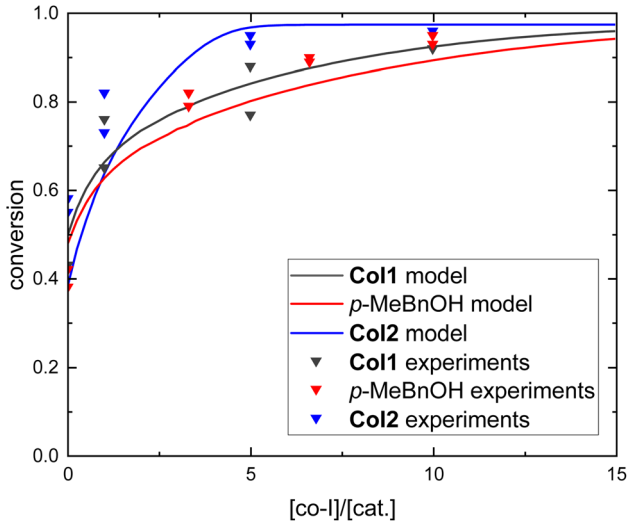

Fig. 9 Influence of co-initiator concentration (as the ratio of co-I to catalyst) for a fixed monomer to catalyst ratio [LA]/[Cat] = 500/1 on conversion after 90 minutes reaction time. Experimental data for *p*-MeBnOH are taken from Conen *et al.*[87] and Fuchs.[89]

It is noteworthy that for co-I ratios of [co-I]/[Cat] < 1, no advantage of the bifunctional co-I is apparent, but further increasing co-I concentrations leads to more strongly increasing conversions. A possible explanation for this is that the equilibrium of activation is not determined by the co-I concentration, but by the concentration of OH groups, and this increases twice as fast for the bifunctional co-I as for the monofunctional co-Is with increasing co-I concentration.

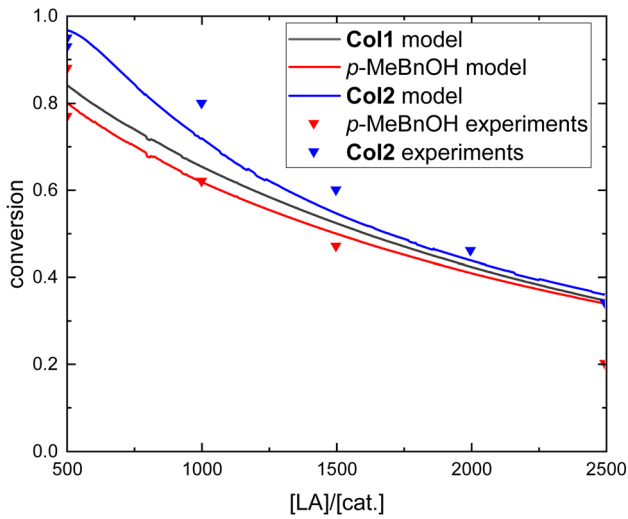

Fig. 10 Influence of catalyst concentration for a fixed co-I to catalyst ratio ([co-I]/[Cat] = 5/1) on conversion after 90 minutes for all co-Is. Experimental data for *p*-MeBnOH are taken from Conen *et al.*[87] and Fuchs.[89]

In this context, it is also interesting to plot the conversion against the catalyst concentration at a constant co-I concentration (see Fig. 10). Here, it can again be seen that only small differences occur for the two monofunctional co-Is. For the bifunctional co-I, on the other hand, the conversions achieved are significantly higher. However, the deviation decreases significantly for lower catalyst concentrations. This can be explained by the fact that for low catalyst concentrations at higher co-I concentrations, the influence of the chain-start by the catalyst is greater and therefore the influence of catalysis by the catalyst residue is higher. Accordingly, the achievable conversions are generally lower, as is the difference between mono- and bifunctional co-Is.

By expanding the existing model to include catalysis of the reaction by catalyst residues and implementing bifunctional co-Is, further steps have been taken towards a deeper understanding of the kinetics of ROP with "asme"-type catalysts. Using a bifunctional co-I, an additional step towards the potential establishment of non-toxic zinc catalysts for industrial polymerizations has been undertaken. The model-based analysis has significantly contributed to the understanding of the chemical relationships and allows conclusions to be drawn about conditions under which bifunctional co-Is can offer particularly large improvements over monofunctional co-Is.

These insights are essential for a successful scale-up in transitioning non-toxic catalysts from academic research to industrial application. The experimental study and model-based analysis presented here serve as important tools for developing a catalyst-co-I system to replace the industrial catalyst tin octoate for a fully sustainable ROP of lactide.

Conclusions

The application of "asme"-type zinc guanidine carboxylate catalysts in the ROP of PLA has been extended to systematically investigate the influence of bifunctional co-initiators. In this study, 1,4-benzenedimethanol was evaluated as a bifunctional co-initiator and benchmarked against the monofunctional counterparts 1-hexanol and *p*-methylbenzyl alcohol. A variety of batch polymerizations were performed using different ratios of lactide to catalyst (ranging from 500 : 1 to 1500 : 1) and co-initiator equivalents (from 1 to 10 with respect to catalyst concentration). Polymerization progress and resulting polymer properties X, M_n and $Đ$ were monitored using *in situ* Raman spectroscopy, NMR spectroscopy and GPC.

Our findings show that the use of both monofunctional and bifunctional co-initiators enables improved control over key polymer properties compared to reactions carried out in the absence of any co-initiator. Increasing the co-initiator concentration generally accelerates the polymerization kinetics, although a plateau in reaction rate is observed beyond a certain threshold. Our previously established kinetic model for the ROP of PLA was expanded to incorporate two critical mechanistic features: (1) the retained catalytic activity of the metal center after ligand dissociation and (2) an additional activation step required for bifunctional co-initiators.

Model predictions for X and $Đ$ show generally good agreement with experimental results. However, some deviations for M_n were noted. The extended model was also used to predict polymerization behavior under conditions not used for

parameter fitting, serving as validation. In these cases, both monofunctional and bifunctional systems exhibited good predictive accuracy, particularly in reproducing conversion and dispersity. Notably, bifunctional co-initiators led to higher conversion overall and are particularly suitable for application with "asme"-type catalysts by reducing the chain initiation by the ligand. Furthermore, at low co-initiator concentrations, catalysis by the deteriorated catalyst becomes increasingly relevant, emphasizing the importance of the model extension introduced in this work.

These findings highlight the versatility of the kinetic model and its applicability in tailoring ROP conditions through judicious choice of co-initiator type and concentration. Ultimately, this contributes to a deeper understanding of zinc guanidine carboxylate-catalyzed ROP while minimizing the experimental effort and paves the way for more efficient and tunable catalyst systems aimed at producing PLA with desired properties under industrially relevant conditions on a larger scale.

Data availability

The data that supports the findings of this study are openly available in RADAR4chem at **https://www.radar-service.eu/radar/en/dataset/qg2e8yckr7kjtj5b?token=ciIcXLyzxVecDszreuQy**.

Conflicts of interest

The authors declare no conflict of interest.

Acknowledgements

The authors thank the Volkswagen foundation for funding the CIRCON project. The authors thank TotalEnergies Corbion bv for lactide donations. Furthermore, the authors would like to thank Prof. Dr Andrij Pich and Marion Conolly from DWI Leibniz Institute Aachen for MALDI Measurements. The authors would further like to thank RADAR4Chem for support and funding of the repository. The open access funding is enabled and organized by Projekt DEAL.

Notes and references

1 S. D. Anuar Sharuddin, F. Abnisa, W. M. A. Wan Daud and M. K. Aroua, *Energy Convers. Manage.*, 2016, **115**, 308–326.
2 N. S. Gurgacz, K. Kvale, M. Eby and A. J. Weaver, *Facets*, 2023, **8**, 1–7.
3 C. M. C. Richard, E. Dejoie, C. Wiegand, G. Gouesbet, H. Colinet, P. Balzani, D. Siaussat and D. Renault, *J. Hazard. Mater.*, 2024, **477**, 135299.
4 J. N. Hahladakis, *Environ. Sci. Pollut. Res.*, 2020, **27**, 12830–12837.
5 T. Iwata, *Angew. Chem., Int. Ed.*, 2015, **54**, 3210–3215.
6 A. Jayakumar, S. Radoor, S. Siengchin, G. H. Shin and J. T. Kim, *Sci. Total Environ.*, 2023, **878**, 163156.
7 R. E. Drumright, P. R. Gruber and D. E. Henton, *Adv. Mater.*, 2000, **12**, 1841–1846.
8 M. J. Stanford and A. P. Dove, *Chem. Soc. Rev.*, 2010, **39**, 486–494.

9 P. McKeown and M. Jones, *Sustainable Chem.*, 2020, **1**, 1–22.
10 S. Jacobsen, H. G. Fritz, P. Degée, P. Dubois and R. Jérôme, *Polym. Eng. Sci.*, 1999, **39**, 1311–1319.
11 O. Dechy-Cabaret, B. Martin-Vaca and D. Bourissou, *Chem. Rev.*, 2004, **104**, 6147–6176.
12 A. Stjerndahl, A. Finne-Wistrand, A.-C. Albertsson, C. M. Bäckesjö and U. Lindgren, *J. Biomed. Mater. Res., Part A*, 2008, **87**, 1086–1091.
13 A. Stjerndahl, A. F. Wistrand and A.-C. Albertsson, *Biomacromolecules*, 2007, **8**, 937–940.
14 A. Buchard, R. H. Platel, A. Auffrant, X. F. Le Goff, P. Le Floch and C. K. Williams, *Organometallics*, 2010, **29**, 2892–2900.
15 N. Yuntawattana, T. M. McGuire, C. B. Durr, A. Buchard and C. K. Williams, *Catal. Sci. Technol.*, 2020, **10**, 7226–7239.
16 F. Fiorentini, W. T. Diment, A. C. Deacy, R. W. F. Kerr, S. Faulkner and C. K. Williams, *Nat. Commun.*, 2023, **14**, 4783.
17 C. Bakewell, A. J. P. White, N. J. Long and C. K. Williams, *Angew. Chem., Int. Ed.*, 2014, **53**, 9226–9230.
18 J. Y. C. Lim, N. Yuntawattana, P. D. Beer and C. K. Williams, *Angew. Chem.*, 2019, **131**, 6068–6072.
19 A. J. Chmura, M. G. Davidson, M. D. Jones, M. D. Lunn, M. F. Mahon, A. F. Johnson, P. Khunkamchoo, S. L. Roberts and S. S. F. Wong, *Macromolecules*, 2006, **39**, 7250–7257.
20 A. J. Chmura, D. M. Cousins, M. G. Davidson, M. D. Jones, M. D. Lunn and M. F. Mahon, *Dalton Trans.*, 2008, 1437–1443.
21 A. Buchard, M. G. Davidson, G. Du Gobius Sart, M. D. Jones, G. Kociok-Köhn, S. N. McCormick and P. McKeown, *Inorg. Chem.*, 2024, **63**, 27–38.
22 O. J. Driscoll, C. K. C. Leung, M. F. Mahon, P. McKeown and M. D. Jones, *Eur. J. Inorg. Chem.*, 2018, **2018**, 5129–5135.
23 J. A. Stewart, P. McKeown, O. J. Driscoll, M. F. Mahon, B. D. Ward and M. D. Jones, *Macromolecules*, 2019, **52**, 5977–5984.
24 J. Beament, M. F. Mahon, A. Buchard and M. D. Jones, *Organometallics*, 2018, **37**, 1719–1724.
25 M. D. Jones, L. Brady, P. McKeown, A. Buchard, P. M. Schäfer, L. H. Thomas, M. F. Mahon, T. J. Woodman and J. P. Lowe, *Chem. Sci.*, 2015, **6**, 5034–5039.
26 J.-C. Buffet and J. Okuda, *Chem. Commun.*, 2011, **47**, 4796–4798.
27 R. Rittinghaus, P. M. Schäfer, P. Albrecht, C. Conrads, A. Hoffmann, A. N. Ksiazkiewicz, O. Bienemann, A. Pich and S. Herres-Pawlis, *ChemSusChem*, 2019, **12**, 2161–2165.
28 R. Rittinghaus, A. Karabulut, A. Hoffmann and S. Herres-Pawlis, *Angew. Chem., Int. Ed.*, 2021, **60**, 21795–21800.
29 R. D. Rittinghaus, J. Zenner, A. Pich, M. Kol and S. Herres-Pawlis, *Angew. Chem., Int. Ed.*, 2022, **61**, e202112853.
30 P. McKeown, S. N. McCormick, M. F. Mahon and M. Jones, *Polym. Chem.*, 2018, **9**, 5339–5347.
31 A. J. Chmura, M. G. Davidson, C. J. Frankis, M. Jones and M. D. Lunn, *Chem. Commun.*, 2008, 1293–1295.
32 F. Santulli, I. D'Auria, L. Boggioni, S. Losio, M. Proverbio, C. Costabile and M. Mazzeo, *Organometallics*, 2020, **39**, 1213–1220.

33 P. McKeown, M. G. Davidson, G. Kociok-Köhn and M. D. Jones, *Chem. Commun.*, 2016, **52**, 10431–10434.
34 O. J. Driscoll, C. H. Hafford-Tear, P. McKeown, J. A. Stewart, G. Kociok-Köhn, M. F. Mahon and M. D. Jones, *Dalton Trans.*, 2019, **48**, 15049–15058.
35 P. V. S. Nylund, B. Monney, C. Weder and M. Albrecht, *Catal. Sci. Technol.*, 2022, **12**, 996–1004.
36 H. Shere, P. McKeown, M. F. Mahon and M. D. Jones, *Eur. Polym. J.*, 2019, **114**, 319–325.
37 V. Vaillant-Coindard, B. Théron, G. Printz, F. Chotard, C. Balan, Y. Rousselin, P. Richard, I. Tolbatov, P. Fleurat-Lessard, E. Bodio, R. Malacea-Kabbara, J. Bayardon, S. Dagorne and P. Le Gendre, *Organometallics*, 2022, **41**, 2920–2932.
38 A. J. Chmura, C. J. Chuck, M. G. Davidson, M. D. Jones, M. D. Lunn, S. D. Bull and M. F. Mahon, *Angew. Chem.*, 2007, **119**, 2330–2333.
39 A. Finne, Reema and A.-C. Albertsson, *J. Polym. Sci., Part A: Polym. Chem.*, 2003, **41**, 3074–3082.
40 H. Ma, T. P. Spaniol and J. Okuda, *Angew. Chem.*, 2006, **118**, 7982–7985.
41 B. J. Jeffery, E. L. Whitelaw, D. Garcia-Vivo, J. A. Stewart, M. F. Mahon, M. G. Davidson and M. D. Jones, *Chem. Commun.*, 2011, **47**, 12328–12330.
42 A. Sauer, A. Kapelski, C. Fliedel, S. Dagorne, M. Kol and J. Okuda, *Dalton Trans.*, 2013, **42**, 9007–9023.
43 S. L. Hancock, M. F. Mahon and M. D. Jones, *Dalton Trans.*, 2013, **42**, 9279–9285.
44 C. Romain, Y. Zhu, P. Dingwall, S. Paul, H. S. Rzepa, A. Buchard and C. K. Williams, *J. Am. Chem. Soc.*, 2016, **138**, 4120–4131.
45 A. D. Schwarz, A. L. Thompson and P. Mountford, *Inorg. Chem.*, 2009, **48**, 10442–10454.
46 M. D. Jones, M. G. Davidson, C. G. Keir, L. M. Hughes, M. F. Mahon and D. C. Apperley, *Eur. J. Inorg. Chem.*, 2009, **2009**, 635–642.
47 S. Ghosh, Y. Schulte, C. Wölper, A. Tjaberings, A. H. Gröschel, G. Haberhauer and S. Schulz, *Organometallics*, 2022, **41**, 2698–2708.
48 H. Shere, P. McKeown, M. F. Mahon and M. D. Jones, *Eur. Polym. J.*, 2019, **114**, 319–325.
49 A. Thevenon, C. Romain, M. S. Bennington, A. J. P. White, H. J. Davidson, S. Brooker and C. K. Williams, *Angew. Chem., Int. Ed.*, 2016, **55**, 8680–8685.
50 M. Fuchs, S. Schmitz, P. M. Schäfer, T. Secker, A. Metz, A. N. Ksiazkiewicz, A. Pich, P. Kögerler, K. Y. Monakhov and S. Herres-Pawlis, *Eur. Polym. J.*, 2020, **122**, 109302.
51 A. Hermann, S. Hill, A. Metz, J. Heck, A. Hoffmann, L. Hartmann and S. Herres-Pawlis, *Angew. Chem., Int. Ed.*, 2020, **59**, 21778–21784.
52 T. Rosen, Y. Popowski, I. Goldberg and M. Kol, *Chem.–Eur. J.*, 2016, **22**, 11533–11536.
53 M. Honrado, A. Otero, J. Fernández-Baeza, L. F. Sánchez-Barba, A. Garcés, A. Lara-Sánchez and A. M. Rodríguez, *Organometallics*, 2014, **33**, 1859–1866.
54 M. Honrado, S. Sobrino, J. Fernández-Baeza, L. F. Sánchez-Barba, A. Garcés, A. Lara-Sánchez and A. M. Rodríguez, *Chem. Commun.*, 2019, **55**, 8947–8950.
55 A. Metz, R. Plothe, B. Glowacki, A. Koszalkowski, M. Scheckenbach, A. Beringer, T. Rösener, J. Michaelis de Vasconcellos, R. Haase, U. Flörke,

A. Hoffmann and S. Herres-Pawlis, *Eur. J. Inorg. Chem.*, 2016, **2016**, 4974–4987.
56 C. Fliedel, V. Rosa, F. M. Alves, A. M. Martins, T. Avilés and S. Dagorne, *Dalton Trans.*, 2015, **44**, 12376–12387.
57 E. D. Akpan, S. O. Ojwach, B. Omondi and V. O. Nyamori, *Polyhedron*, 2016, **110**, 63–72.
58 C. K. Williams, L. E. Breyfogle, S. K. Choi, W. Nam, V. G. Young, M. A. Hillmyer and W. B. Tolman, *J. Am. Chem. Soc.*, 2003, **125**, 11350–11359.
59 C. C. Roberts, B. R. Barnett, D. B. Green and J. M. Fritsch, *Organometallics*, 2012, **31**, 4133–4141.
60 D. Jędrzkiewicz, G. Adamus, M. Kwiecień, Ł. John and J. Ejfler, *Inorg. Chem.*, 2017, **56**, 1349–1365.
61 A. Otero, J. Fernández-Baeza, L. F. Sánchez-Barba, S. Sobrino, A. Garcés, A. Lara-Sánchez and A. M. Rodríguez, *Dalton Trans.*, 2017, **46**, 15107–15117.
62 N. M. Rezayee, K. A. Gerling, A. L. Rheingold and J. M. Fritsch, *Dalton Trans.*, 2013, **42**, 5573–5586.
63 Z. Dai, J. Zhang, Y. Gao, N. Tang, Y. Huang and J. Wu, *Catal. Sci. Technol.*, 2013, **3**, 3268.
64 D. J. Darensbourg and O. Karroonnirun, *Macromolecules*, 2010, **43**, 8880–8886.
65 C. Fliedel, D. Vila-Viçosa, M. J. Calhorda, S. Dagorne and T. Avilés, *ChemCatChem*, 2014, **6**, 1357–1367.
66 Y. Sun, Y. Cui, J. Xiong, Z. Dai, N. Tang and J. Wu, *Dalton Trans.*, 2015, **44**, 16383–16391.
67 J. E. Chellali, A. K. Alverson and J. R. Robinson, *ACS Catal.*, 2022, **12**, 5585–5594.
68 P. McKeown, J. Brown-Humes, M. G. Davidson, M. F. Mahon, T. J. Woodman and M. D. Jones, *Dalton Trans.*, 2017, **46**, 5048–5057.
69 S. P. Bassett, A. D. Russell, P. McKeown, I. Robinson, T. R. Forder, V. Taresco, M. G. Davidson and S. M. Howdle, *Green Chem.*, 2020, **22**, 2197–2202.
70 S. Ghosh, P. M. Schäfer, D. Dittrich, C. Scheiper, P. Steiniger, G. Fink, A. N. Ksiazkiewicz, A. Tjaberings, C. Wölper, A. H. Gröschel, A. Pich, S. Herres-Pawlis and S. Schulz, *ChemistryOpen*, 2019, **8**, 951–960.
71 P. Steiniger, P. M. Schäfer, C. Wölper, J. Henkel, A. N. Ksiazkiewicz, A. Pich, S. Herres-Pawlis and S. Schulz, *Eur. J. Inorg. Chem.*, 2018, **2018**, 4014–4021.
72 Z. Zhong, P. J. Dijkstra and J. Feijen, *Angew. Chem.*, 2002, **114**, 4692–4695.
73 A. Hermann, T. Becker, M. A. Schäfer, A. Hoffmann and S. Herres-Pawlis, *ChemSusChem*, 2022, **15**, e202201075.
74 P. M. Schäfer, M. Fuchs, A. Ohligschläger, R. Rittinghaus, P. McKeown, E. Akin, M. Schmidt, A. Hoffmann, M. A. Liauw, M. Jones and S. Herres-Pawlis, *ChemSusChem*, 2017, **10**, 3547–3556.
75 P. M. Schäfer, P. McKeown, M. Fuchs, R. Rittinghaus, A. Hermann, J. Henkel, S. Seidel, C. Roitzheim, A. N. Ksiazkiewicz, A. Hoffmann, A. Pich, M. Jones and S. Herres-Pawlis, *Dalton Trans.*, 2019, **48**, 6071–6082.
76 P. M. Schäfer and S. Herres-Pawlis, *ChemPlusChem*, 2020, **85**, 1044–1052.
77 K. A. George, F. Schué, T. V. Chirila and E. Wentrup-Byrne, *J. Polym. Sci., Part A: Polym. Chem.*, 2009, **47**, 4736–4748.
78 A. Amgoune, C. M. Thomas and J.-F. Carpentier, *Macromol. Rapid Commun.*, 2007, **28**, 693–697.

79 R. D. Rittinghaus, J. Zenner, A. Pich, M. Kol and S. Herres-Pawlis, *Angew. Chem., Int. Ed.*, 2022, **61**, e202112853.
80 B. Théron, V. Vaillant-Coindard, C. Balan, Y. Rousselin, J. Bayardon, R. Malacea-Kabbara and P. Le Gendre, *Dalton Trans.*, 2023, **52**, 7854–7868.
81 J. Payne, P. McKeown, M. F. Mahon, E. A. C. Emanuelsson and M. Jones, *Polym. Chem.*, 2020, **11**, 2381–2389.
82 S. D'Aniello, S. Laviéville, F. Santulli, M. Simon, M. Sellitto, C. Tedesco, C. M. Thomas and M. Mazzeo, *Catal. Sci. Technol.*, 2022, **12**, 6142–6154.
83 D. Bandelli, C. Weber and U. S. Schubert, *Macromol. Rapid Commun.*, 2019, **40**, e1900306.
84 T. Rosen, I. Goldberg, W. Navarra, V. Venditto and M. Kol, *Angew. Chem., Int. Ed.*, 2018, **57**, 7191–7195.
85 R. Hador, M. Shuster, V. Venditto and M. Kol, *Angew. Chem., Int. Ed.*, 2022, **61**, e202207652.
86 Y. Zhou, G. S. Nichol and J. A. Garden, *Eur. J. Inorg. Chem.*, 2022, **2022**, e202200134.
87 N. Conen, M. Fuchs, A. Hoffmann, S. Herres-Pawlis and A. Jupke, *Adv. Sustainable Syst.*, 2023, 2200359.
88 A. Kowalski, A. Duda and S. Penczek, *Macromolecules*, 1998, **31**, 2114–2122.
89 M. Fuchs, *Zur Nutzung von N,O-Hybridguanidin-Zink-Komplexen als multifunktionale Katalysatoren zur Implementierung einer biobasierten Kunststoffkreislaufwirtschaft*, RWTH Aachen University, 2024.
90 G. Schwach, J. Coudane, R. Engel and M. Vert, *Polym. Bull.*, 1996, **37**, 771–776.
91 Y. Yu, E. J. Fischer, G. Storti and M. Morbidelli, *Ind. Eng. Chem. Res.*, 2014, **53**, 7333–7342.
92 Y. Yu, G. Storti and M. Morbidelli, *Macromolecules*, 2009, **42**, 8187–8197.
93 Y. Yu, G. Storti and M. Morbidelli, *Ind. Eng. Chem. Res.*, 2011, **50**, 7927–7940.
94 S. Metkar, V. Sathe, I. Rahman, B. Idage and S. Idage, *Chem. Eng. Commun.*, 2019, **206**, 1159–1167.
95 P. Pladis, K. Karidi, T. Mantourlias and C. Kiparissides, *Macromol. React. Eng.*, 2014, **8**, 813–825.
96 F. Weng, X. Li, Y. Wang, W.-J. Wang and S. J. Severtson, *Macromol. React. Eng.*, 2015, **9**, 535–544.
97 A. Zubov and G. Sin, *Chem. Eng. J.*, 2018, **336**, 361–375.
98 D. R. Witzke, *Introduction to properties, engineering and prospects of polylactide polymers*, Michigan State University, 1997.
99 H. M. Hulburt and S. Katz, *Chem. Eng. Sci.*, 1964, **19**, 555–574.
100 R. P. Rosa, F. V. Ferreira and L. M. F. Lona, *Chem. Eng. Sci.*, 2021, **246**, 116934.
101 I. Zapata-González and E. Saldívar-Guerra, *Can. J. Chem. Eng.*, 2023, **101**, 5324–5356.